2018

An Improved Numerical Method for Assessing Cell Elasticity from Atomic Force Microscopy Nanoindentation Data

Jared Alexander Feindt
Lehigh University

An Improved Numerical Method for Assessing Cell Elasticity from Atomic Force Microscopy Nanoindentation Data

by

Jared Feindt

Presented to the Graduate and Research Committee

of Lehigh University

in Candidacy for the Degree of

Master of Science

in

Mechanical Engineering and Mechanics

Lehigh University

December 2017

Thesis is accepted and approved in partial fulfillment of the requirements for the Master of Science in Mechanical Engineering.

An Improved Numerical Method for Assessing Cell Elasticity from Atomic Force Microscopy Nanoindentation Data.

_____

Date Approved

_____

Prof. Hannah Dailey, Thesis Advisor

_____

Prof. D. Gary Harlow, Chairperson
of Department of Mechanical
Engineering and Mechanics

Acknowledgements

I would first and foremost like to thank my research advisor Dr. Hannah Dailey for providing me with the much needed guidance to complete my Master's Thesis. Her knowledge in modeling, finite element analysis, and extensive background in the bioengineering field has greatly improved my research skills and prepared me for any engineering challenges I might face in the future.

I would also like to thank Dr. Matthew Dragovich, who spent many hours with me explaining the intricacies of the experimental and computational challenges associated with collecting data with Atomic Force Microscopy. Additionally, I would like to thank Dr. Frank Zhang for his help in leading the BDSI 2016 and 207 summer research groups with my advisor, Hannah Dailey. I would also like to thank Wenpeng Cao, who helped collect data in the BDSI 2017 summer research group.

Table of Contents

List of Figures

Abstract

This work presents a new numerical method for processing atomic force microscopy (AFM) data to determine the elasticity of cultured adherent biological cells. Raw AFM force-indentation data is commonly interpreted using the Hertz and Sneddon contact mechanics models to fit a Young's modulus or apparent cell elasticity. This apparent cell elasticity is highly dependent on the method used to identify the first point of contact between the AFM probe and the cell surface. In this work, an automated MATLAB-based data processing algorithm was developed to detect the point of probe-cell contact in the force-indentation curve. The method handles the difficulties associated with finding the contact point using moving averages, thresholds, and mean squared errors. Implementation validation shows that contact point detection accuracy is critical, with seemingly small errors producing up to 250% changes in reported elasticity within a single experiment.

The newly developed method was applied to analyze a large experimental data series with human pancreatic adenocarcinoma (AsPC-1) cells. The results from this test series show that pyramidal AFM probes systematically measure elasticities that are a factor of three greater than those measured by spherical probes. Across a range of typically used probe forces, increasing the indentation force results in a 100% increase in apparent elasticity. Finally, the results of the new data processing method show that accurate contact point detection and data quality checking eliminates the log-normal distribution of elasticity values that is often reported in experimental AFM studies with biological cells.

These findings showcase the importance of including detailed descriptions of data processing methods and the need for robust analysis algorithms in AFM research.

Keywords

Atomic force microscopy, numerical modeling, data processing, cell mechanics, classical contact mechanics, nanoindentation, cancer, force-indentation curve

Introduction

During the normal course of growth and development, living biological cells undergo phenotypic differentiation, transforming their morphology, structure, and mechanical properties to achieve a form that is adapted for a specific purpose. Typically, these specialized cell types self-replicate until organism death, but sometimes DNA mutations or replication errors can produce cells that initiate diseases such as cancer, in which unchecked cell growth and malignant invasion into other tissues can damage organ systems and lead to death.

Recent advances in cancer research have included attempts to characterize the changes that arise in cancerous compared to non-cancerous cells, including differences in mechanical properties at the cellular level that could be useful for diagnostic purposes[1–3]. Many methods have been used to estimate cellular mechanical properties with the goal of learning more about their underlying mechanical properties and their correlation with disease[2,4–9]. One commonly-used experimental technique for probing cell mechanics is atomic force microscopy (AFM) nanoindentation (see **Figure 1**). Raw data collected via AFM nanoindentation is often interpreted using equations derived from classical contact mechanics models to estimate the Young's modulus of cells[10]. In the AFM nanoindentation literature, it has been commonly reported that higher indentation forces and indentation depths result in systematically higher apparent cell elasticities[11,12]. These higher apparent elasticities have been attributed to substrate effects and the structural differences between the cell's surface and the cell's interior components. Another common finding is that cells indented with pyramidal probes present higher apparent elasticities than those indented

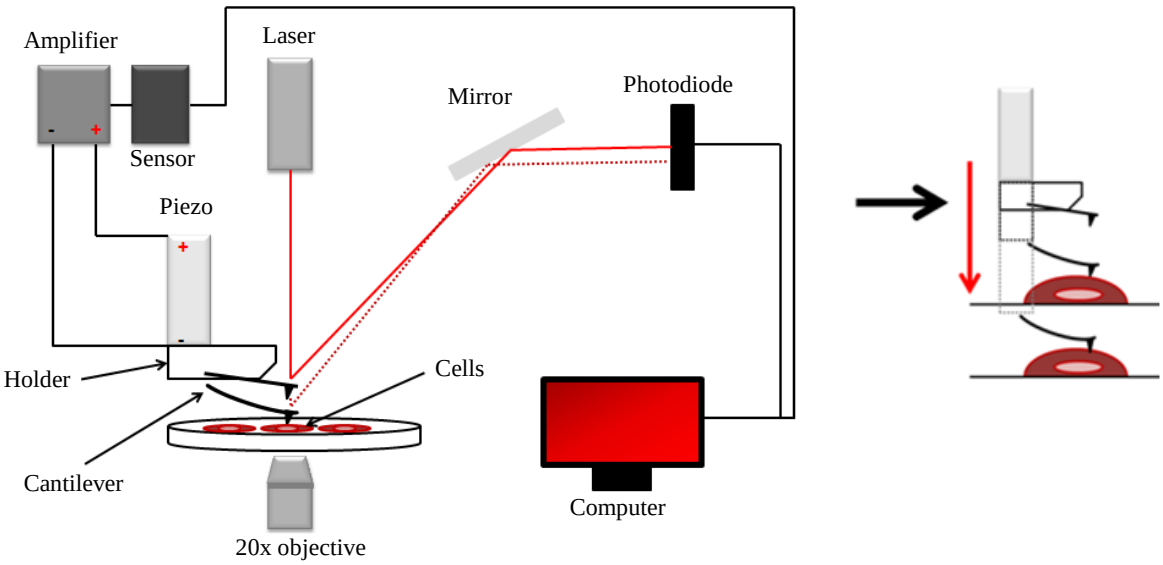

Figure 1: Schematic diagram of custom-built AFM (left) and a single-cell nanoindentation (right).

with spherical probes[12]. This has been attributed to limitations in the Sneddon model, higher uncertainty of contact point due to the smaller indentation area, and the higher probability of measuring local elasticity rather than a bulk measurement. However, the published works from different research groups have used different data processing algorithms to fit cell elasticity values and these inconsistencies are not always transparently reported and clearly discussed.

In view of the persistent challenges pertaining to analysis of AFM nanoindentation data analysis, the objective of this work was to develop a robust new method for analyzing AFM data to accurately determine when the probe contacts the surface of the cell. This thesis presents an overview of essential concepts for understanding AFM nanoindentation data and lays out a new method for numerical analysis and parameter fitting. To test the efficacy of the newly developed analysis method, AFM nanoindentation data sets for biological cells under various experimental conditions were processed and analyzed. Specifically, human pancreatic cancer (AsPC-1) cells were indented with target forces of

100, 300, 600, and 1000pN and indentation speeds of 0.94, 1.88, 3.76, and 7.52 μm/s using both spherical and pyramidal probes on collagen-coated polystyrene. This range of conditions provided data sets with a variety of challenges that are characteristic of AFM nanoindentation experiments carried out by many investigator groups.

The overall goal of this work was to identify pitfalls in AFM nanoindentation data analysis, present a method for processing data to avoid these errors, and make a set of universal recommendations for data processing and reporting of results that may be useful to others in the field. By documenting, sharing, and refining detailed methods used to determine fitted parameters from experimental data, researchers may be able to achieve more standardization between groups. This may enable more useful comparisons between data sets and more rapid advancement of knowledge in the field as a whole.

Methods

Data Source: Atomic Force Microscopy (AFM) Nanoindentation Experiments

The numerical method presented in this work is specifically adapted for processing raw data from atomic force microscopy (AFM) nanoindentation experiments. During a nanoindentation scan, the AFM tip travels vertically towards the cell surface. Upon indentation of the cell, the AFM cantilever acts like a soft spring of known spring constant, which is calculated in a calibration step before the experiment begins. The cantilever deflection is measured and recorded together with the force at every sampling point. The slope of the resulting force-indentation curve directly reflects the cell stiffness (expressed in [pN/μm]), but can be converted to an apparent material elastic stiffness, E, in [Pa] by means of equations derived from classical contact mechanics for a sphere (Hertz equation)

or cone (Sneddon equation) in contact with a semi-infinite medium. A detailed schematic of the AFM experimental setup can be found in **Appendix A**.

A typical cell characterization experiment involves repeating 20 individual force-indentations per cell for 40 cells, or a total of roughly 800 raw data sets from which cell mechanical properties are to be inferred. Validation data for this thesis consists of 14 experimental groups or a total of approximately 11,200 force-indentation curves requiring analysis.

Data Processing Theoretical Model: Hertz and Sneddon Contact Mechanics Equations

In addition to his contributions in other fields, Heinreich Hertz established the field of contact mechanics in 1882[13]. In his paper, he proposed the Hertz model for describing elastic contact between an elastic sphere and an elastic half-space. Over 80 years later in 1965, Ian Sneddon proposed a model for contact between a rigid cone and an elastic half-space[14]. Both the Hertz and Sneddon contact models assume:

1. The strains are small and within the elastic limit.
2. The surfaces are continuous and non-conforming, meaning that the contact area is much smaller than the dimensions of the bodies present.
3. The contacted body can be considered an elastic semi-infinite half-space.
4. The surfaces are frictionless.

After using these assumptions, the elasticity can be calculated using equation 1 for a spherical probe, or equation 2 for a pyramidal probe.

$$E_{app} = \frac{3}{4}\frac{(1-\nu^2)F}{R^{1/2}d^{3/2}} \quad (1)$$

$$E_{app} = F\pi\frac{(1-\nu^2)\tan\theta}{2d^2} \quad (2)$$

Where E_{app} is the apparent elasticity, F is the indentation force, ν is the cell's viscocity (0.49), R is the radius of the probe ($5\mu m$), d is the indentation depth, and θ is the angle between the outside of the probe and the semi-infinite surface. Derivations for these equations can be found in **Appendix B**.

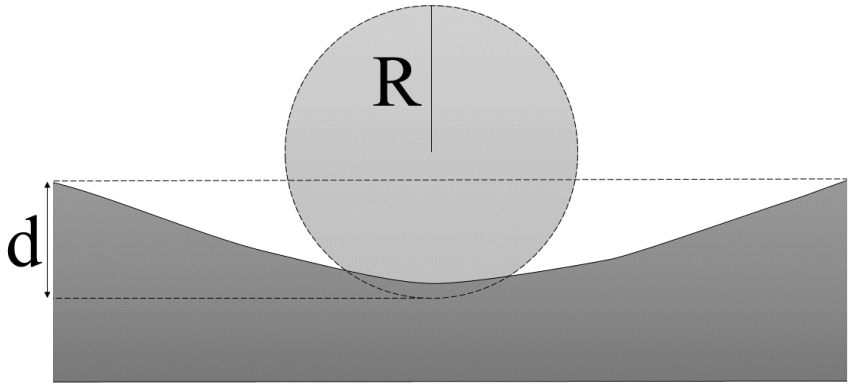

Figure 2: Spherical probe contacting semi-infinite half space in the Hertz model. Dotted line indicates contact.

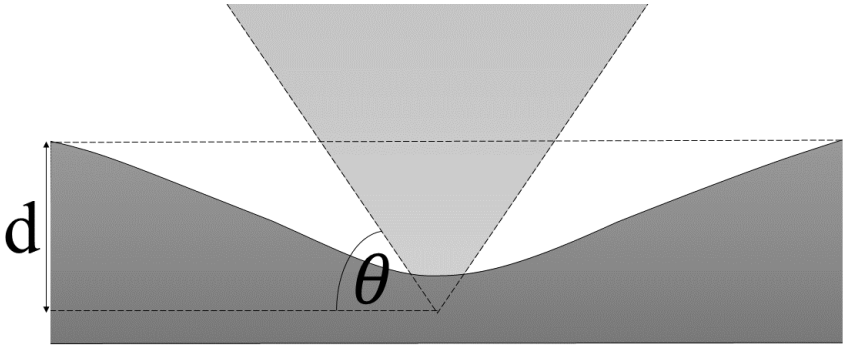

Figure 3: Conical probe indenting semi-infinite half space in the Sneddon model, where θ represents the angle between the half-space surface and the outside of the cone. Dotted line indicates indentation.

The Hertz and Sneddon models have been widely adopted for use in interpreting force-indentation curves from experimental AFM studies, despite some notable violations of the assumptions. These models assume small strains, small contact area, a semi-infinite contact body, and frictionless contact, which are all commonly violated in AFM characterization of cell mechanics. A more thorough description of these assumptions can

be found in **Appendix B**. Notably, the most common type of AFM probe is pyramidal in shape, but is often fit using the Sneddon model assuming a conical shape of equivalent contact angle, θ (see **Figure 3**).

Data Processing Implementation in MATLAB

In this work, a MATLAB (v. 2017a, The MathWorks, Inc., Natick, MA) algorithm was developed to process the raw data from AFM experiments. The MATLAB code comprises a suite of functions that carry out the following tasks: navigate to the folders that contain the data files, import the Igor Pro (*.ibw) files to MATLAB variables ("IBWread, Bialek 2009, MathWorks), and then execute a newly developed numerical method for processing the data to fit an apparent material Young's modulus, E, for each force-indentation curve. The code also exports a graphical rendering of the data for each force-indentation curve, with the tip contact location indicated and an overlay of the best-fit curve used by the code to assign a value for E (see representative example, **Figure 4**).

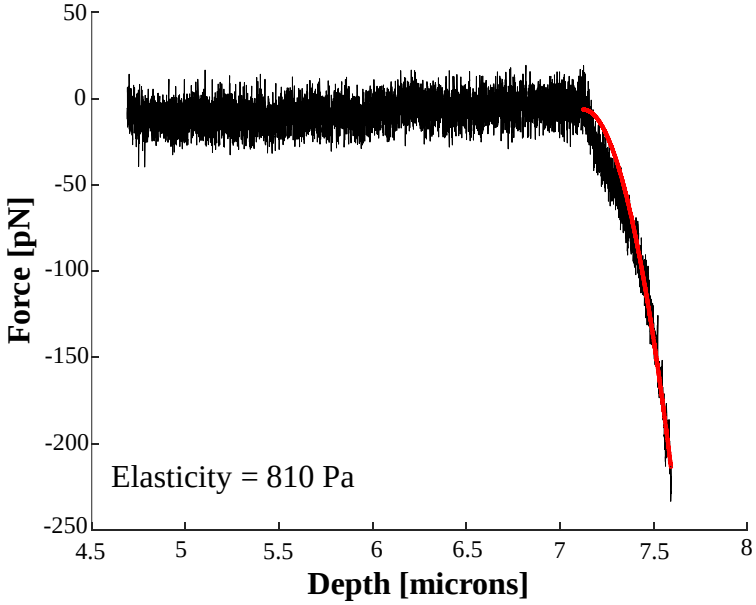

Figure 4: Sample force-indentation data with a Hertz fit from the tip-surface contact point identified by the MATLAB algorithm.

After the data for a given force-indentation curve has been loaded by the code, it must be processed to detect the first point of contact between the tip and the material surface. This point defines the start of the section of the force-indentation data that must be used to fit an apparent elasticity, *E*, but is difficult to detect in the raw data state due to the characteristic noise observed in the data. Accordingly, the first step in contact point detection is to perform a smoothing operation on the raw data using a 200-point moving average method applied twice in succession. This produces the smoothed curve shown in red in **Figure 5**, which has thermal oscillations in the approach curve (non-contacting region) and a clear turning point at the start of the indentation curve (contact region).

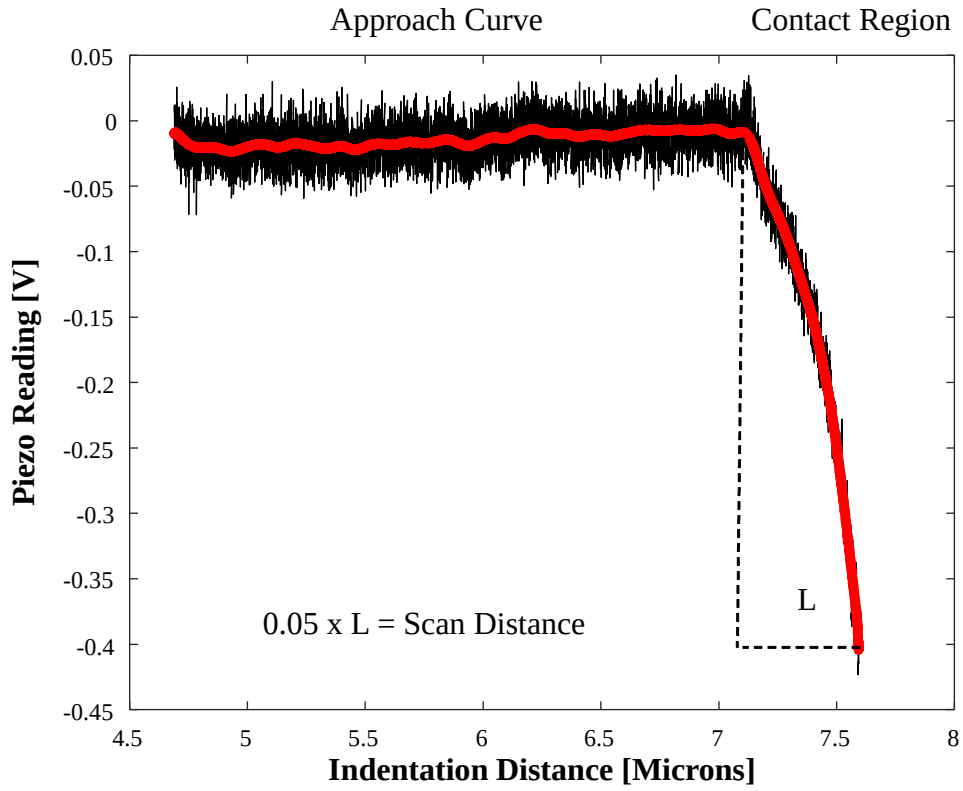

Figure 5: Raw data as exported from the AFM system for a representative force-indentation curve for a spherical probe contacting an AsPC-1 cell in the nuclear region. Black lines indicate raw data and red overlay represents the smoothed curve generated by the MATLAB code.

After the data has been smoothed, all local minima and maxima of the smoothed data are recorded (**Figure 6**). Next, the code starts from the maximum force recorded and works backward, checking whether each local maximum is part of the approach curve or represents a local deviation in the contact curve. To check this, each local maximum is compared to a defined threshold relative to the maximum force value of the smoothed data. If a given local maximum is within the defined threshold, then it is considered part of the approach curve. If a given local maximum is outside the defined threshold, then it is considered a part of the contact curve and the code moves on to the previous local maximum and repeats the threshold-checking process. The threshold for local maxima checking was selected for each experimental condition based on the expected ratio of the maximum indentation depth to the magnitude of the thermal noise oscillations. The chosen threshold for local maxima checking was 15% for most experimental conditions, but visual inspection of some cell lines showed that 15% was too high for very low-force loading cases. In these cases, a 10% or 7% threshold was used. This threshold also allows

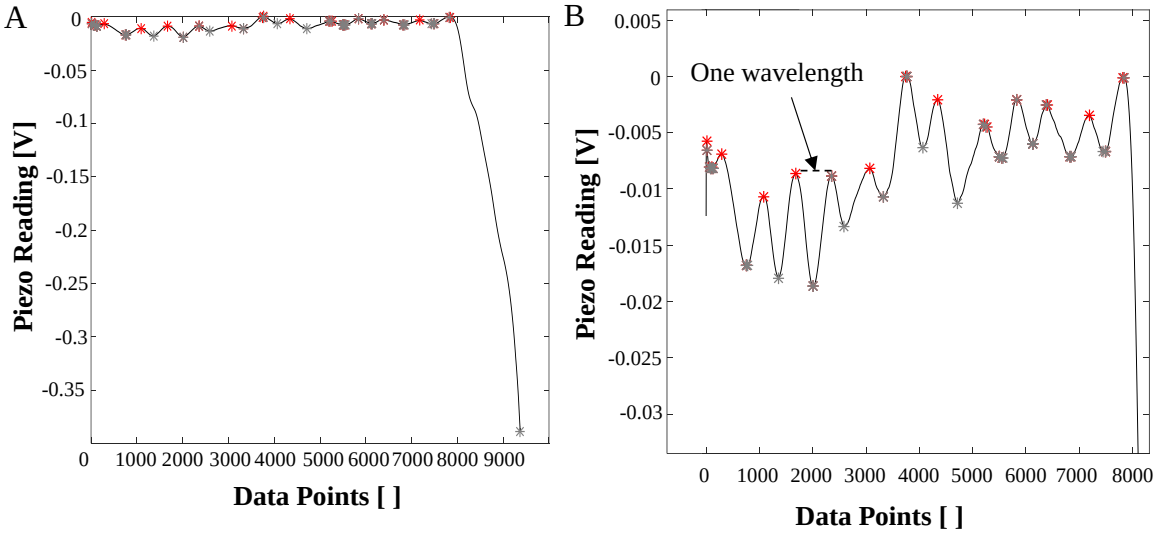

Figure 6: A) Smoothed raw data. B) Zoomed-in region of the smoothed data showing local minima and maxima in the pre-contact region. These points are used to calculate the characteristic thermal wavelength.

preliminary data quality screening. Generally, this threshold is not reached if the data is nonphysical (e.g. unexplained high levels of noise, optical interference in the photodetector, no contact achieved for a given scan, or contact achieved only with the dish, not a cell). In any of these cases, the scan is discarded, as slight changes in contact point choice and in contact region noise cause large changes in inferred elasticity (**Figure 7**).

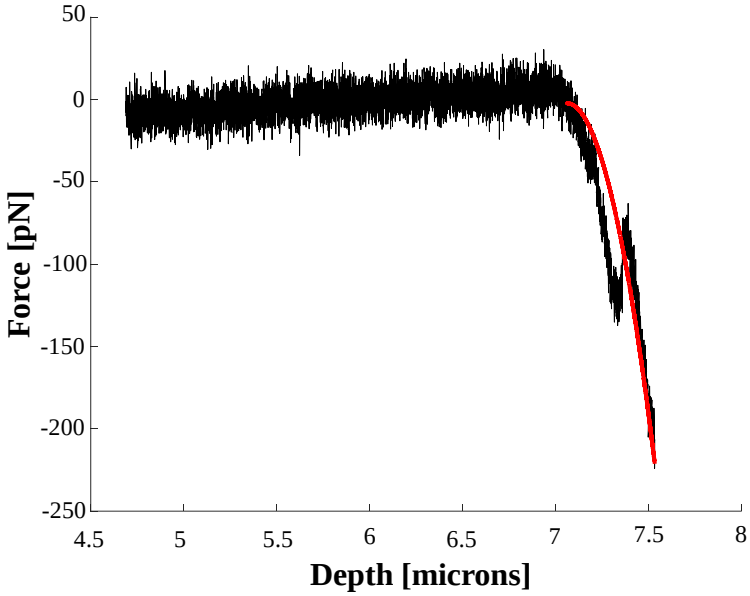

Figure 7: A scan with nonphysical data in the contact region that is manually or automatically discarded.

The result of the local maxima threshold checking process is to define a point in the data that is near the start of the tip-surface contact region. Using this point as a cutoff, the code looks backward in the data set and calculates a characteristic "thermal noise wavelength" by taking the median of the distances between local maxima (**Figure 8**). At 1/8 of a wavelength past the first local maximum that meets the threshold, the code begins looking for the correct tip-surface contact point. This process involves calculation of the local slope change over a small segment of the indentation curve. In this small segment of the data, if the local slope increases above a specified threshold, this data point defines the tip-surface contact location. The distance over which the slope is calculated is defined as a new variable, "Scan Distance", which is set to 5% of the data remaining after the local maximum chosen as the near-contact point (**Figure 8).**

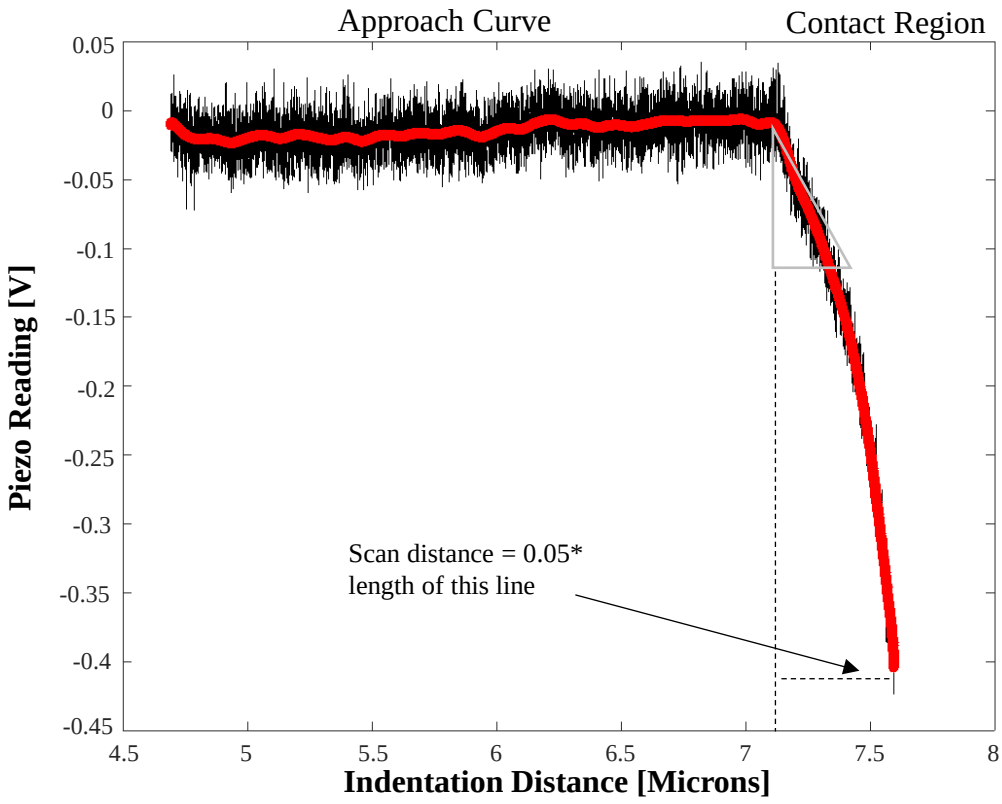

Figure 8: Contact point detection involves sequential calculation of the local slope in the region of interest based on a parameter called scan distance, or 5% of the length of the horizontal dotted line shown. The length of the bottom side of the gray triangle is equal to scan distance, but the triangle is enlarged for this image. The triangle represents the theta threshold for the included angle. If the local slope falls within this triangle, it passed the slope threshold test and the apex of the triangle is stored as the tip-surface contact point. If the local slope is too shallow, the apex of the triangle is not the tip-surface contact point and the code will advance to the next data point and repeat the checking process. The first point checked is 1/8 of a thermal wavelength after the last local maximum, with the thermal wavelength and all local maxima being shown in Figure 6.

To calculate a local slope at the candidate tip-surface contact point, the code records the difference in X and Y values between the current point and a data point "Scan Distance" further into the contact region. If the included angle of these two points is above a certain threshold (again, dependent on the cell line), the first point of contact between the AFM tip and the cell has been found. If the slope threshold criteria is not met, the code will advance to the next data point and check again. If no data point on the contact curve passes

the slope threshold test, the code reports an error and the scan is discarded. This "angle threshold" method that is used is the motivation for looking at 1/8 of a wavelength after the chosen maximum, rather than at the chosen maximum. If the code started looking at the local maximum, the included angle is likely to be higher. If the code starts at 1/2 wavelength after the contact point, it might assign the contact point too late.

With the tip-surface contact point now known, the next step is to fit a constitutive relation that will allow definition of the apparent material Young's modulus, *E*, by a least squares fit to the contact region data. To do this, the contact region of the raw, not smoothed, data is fit using a MATLAB built-in least squares fitting function (nlinfit) with the appropriate contact equation, either Hertz or Sneddon (Equation 1 or 2), depending on the tip type. A sample contact-region curve fit is shown in **Figure 9**. An image of this fit is then saved as a *.png file for subsequent visual checking to make sure that an appropriate contact point was selected and that the force-indentation curve does not need to be discarded due to non-physical behavior.

The code performs the above procedure on all force-indentation curves for a particular cell, recording all elasticities, maximum forces, and

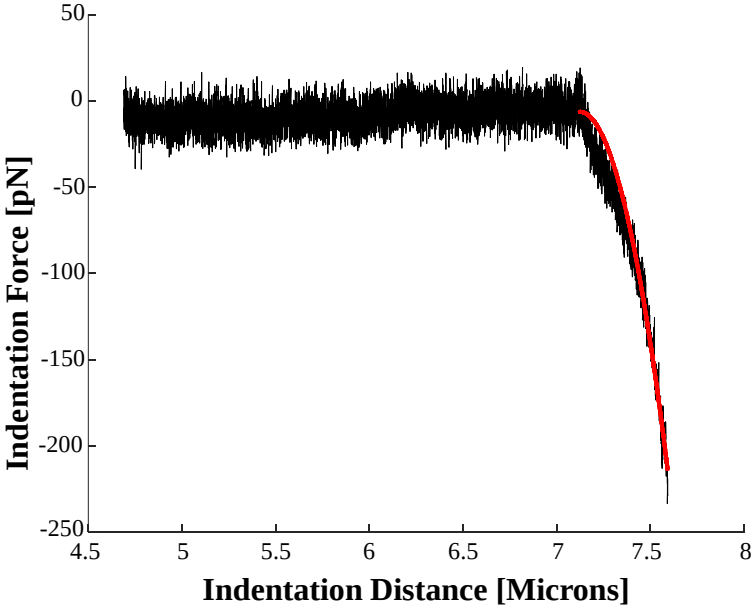

Figure 9: Sample force-indentation data with a Hertz fit from the tip-surface contact point identified by the MATLAB algorithm.

maximum indentation depths found for each force-indentation curve. Occasionally, a force-indentation data set may have non-physical behavior or other unusual features that cause the automatic tip-surface contact point detection to fail. In these cases, the scan is flagged for visual review and a tool is launched to allow the user to manually click to select the contact point using the graphical user interface. In a typical set of 800 scans for a single cell line at a given set of AFM operating parameters, approximately 20 of these (2.5%) are non-physical and need to be thrown out, and 10 (1.25%) are valid scans that have unusual or challenging features in the force-indentation curve and therefore require manual contact point selection. After all of the analysis and quality checking is complete, a summary value for each cell is generated by calculating the median values for each cell's set of curves. These medians are then recorded for subsequent statistical analysis and reporting. An archived copy of the source code used in this work is included as a supplemental file.

Results Processing and Statistics

Data output from MATLAB (median elasticity, peak indentation force, and indentation depth) for each cell was processed in Microsoft Excel for plotting. Statistical analysis was carried in IBM SPSS Statics 24 (IBM Corp, Armonk, NY). Normality was checked by Kolmogorov-Smirnov and Shapiro-Wilk testing and reviewing Q-Q plots. Distributions of apparent cell elasticity tended to be normally distributed in most groups, with a few moderate violations of normality. Accordingly, differences between groups were checked using analysis of variance (one-way and two-way ANOVA), which tends to be robust to violations of normality assumptions.

Results

Data Processing Parameter Selection and Sensitivity – Test Case Analysis

To test the sensitivity of the numerical method to changes in the parameters used for contact point detection, a test data set was evaluated under three conditions: contact point detected too early, correctly, and too late. To select the contact point early, the local slope threshold, ϕ, was set to 10° and the local maximum threshold was set to 5%. To select the contact point correctly, ϕ was set to 20° and the local maximum threshold was set to 10%. To select the contact point late, ϕ was set to 40° and the local maximum threshold was set to 12%. These parameters were chosen after visually verifying that each set of parameters produced Hertz fits that appeared equal, despite giving different apparent elasticity measurements. Larger adjustments to these parameters would have resulted in egregiously incorrect Hertz fits. The results showed that selection of contact point has a significant influence on apparent elasticity ($p < 0.001$ by one-way ANOVA testing) (see **Figure 10**).

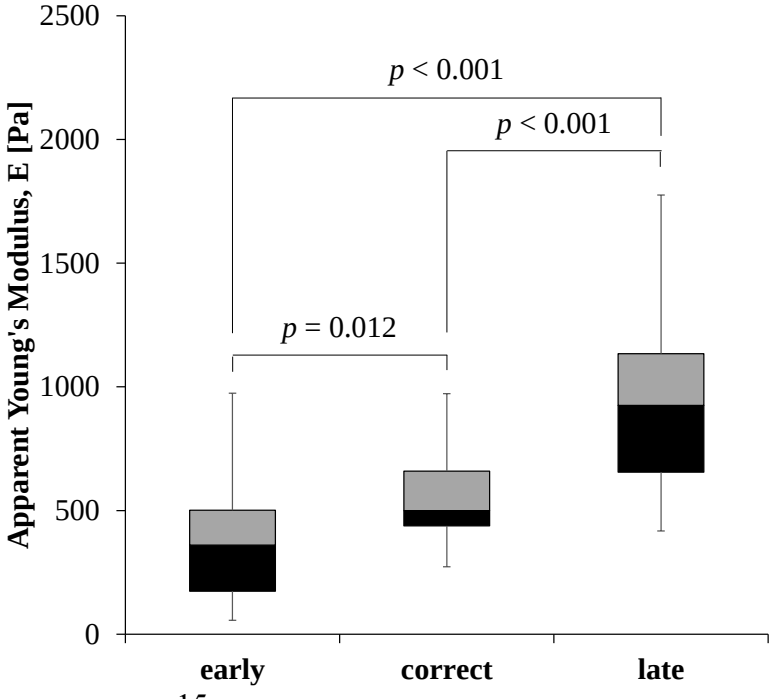

Figure 10: The AFM data processing code was adapted to test the impact of selecting the contact point deliberately too early and too late. Picking the contact point too late resulted in significantly higher apparent stiffness.

A closer examination shows that with these early-correct-late variations, the contact point moves only slightly, but this greatly affects the Hertz-derived apparent elasticities (**Figure 11**). In the method developed for this work, contact point selection was dependent on the thresholds used for local slope change detection. For some force-indentation curves, changes to the local slope and local maximum thresholds results in no change in contact point selection (**Figure 11, A-C**). For others, changes to the local slope and local maximum thresholds result in selecting the contact point early (**Figure 11, G**) or late (**Figure 11, F&I**). Picking seemingly equivalent contact points can easily result in a 20% difference in apparent elasticity for a single indentation.

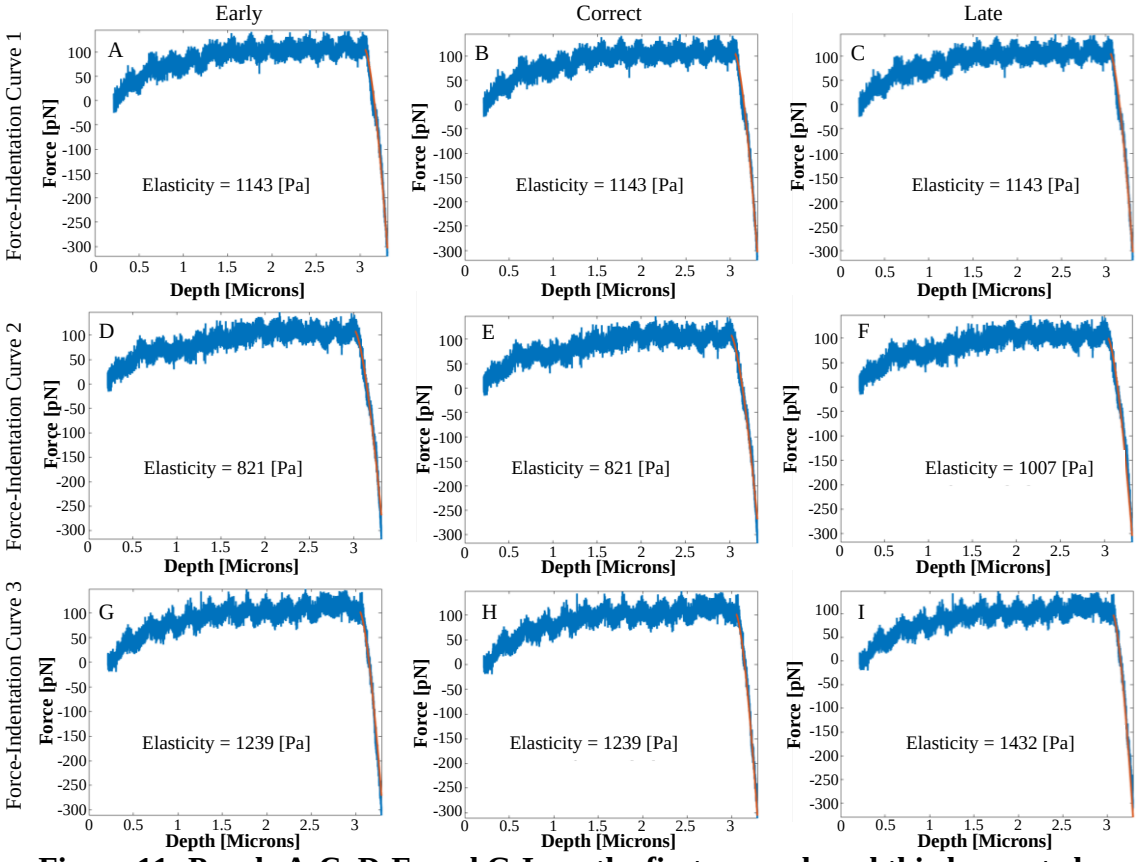

Figure 11: Panels A-C, D-F, and G-I are the first, second, and third repeated indentations of the same three cells. The first, second, and third column show results from changing contact point detection parameters. These changes sometimes result in picking the contact point early, late, or result in no change, which directly affects apparent elasticity.

Algorithm Application to Experimental AFM Data

To test the robustness of the algorithm for contact point detection and cell elasticity analysis, a challenging large data set was processed using the new code. This data consisted of a variety of experimental conditions corresponding to the range of typically used parameters in the published AFM literature, including variations in tip shape, piezo speed, and tip force. These variations produced raw data with variable signal to noise ratio and a variety of other challenging features.

The first experimental variation considered was the effect of piezo speed for two tip types (sphere and pyramid), as shown in **Figure 12**. A two-way ANOVA showed that pyramidal probe-derived apparent elasticity measurements were significantly higher than spherical estimates ($p < 0.001$) and about 3 times higher on average with the pyramidal probe compared to the sphere. There was no statistically significant effect of indentation speed, but a few individually significant pairings indicated in **Figure 12**. These trends and statistically significant pairings mirrored those found in the different applied indentation

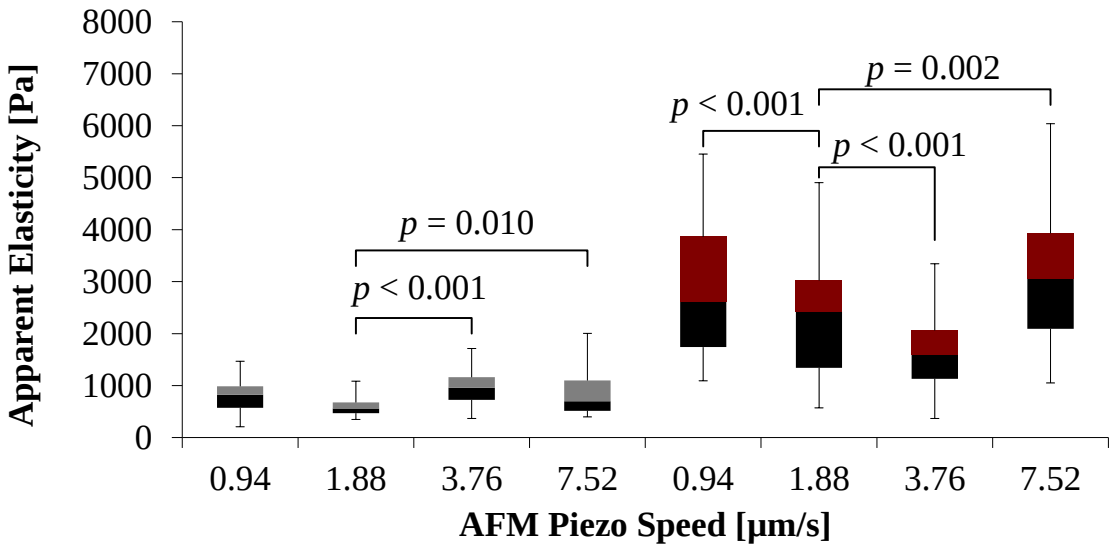

Figure 12: Dependence of elasticity and indentation depth on indentation speed at 300 pN for spherical (left) and pyramidal (right) probes.

forces between these groups despite having the same force targets (**Figure 13**). This data indicated that across the range of speeds used, the AFM system had systematic variations in indentation force at each speed and that interpretation of the speed data requires examination of the effect of indentation force on apparent cell elasticity.

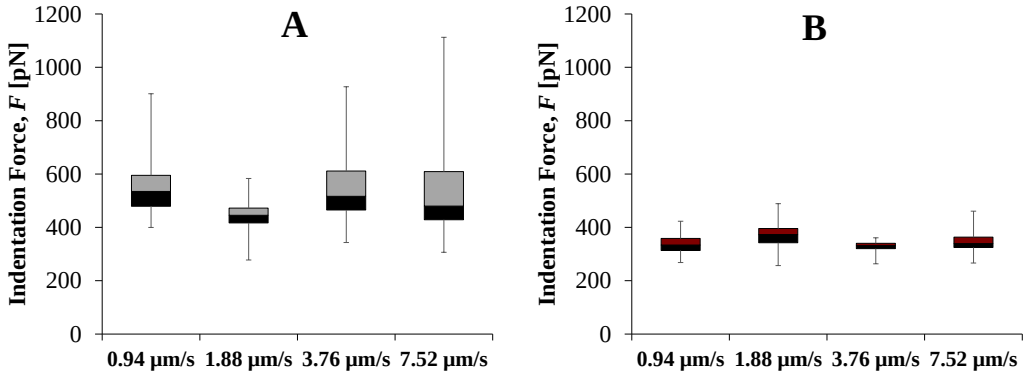

Figure 13: Force distributions for spherical (A) and pyramidal (B) indentations with 300 pN target forces.

The next experimental parameter examined was tip force, again with both spherical and pyramidal tips (see **Figure 14**). Overall, apparent cell elasticity significantly increased with increasing indentation force ($p < 0.001$ overall). Two-way ANOVA again showed that cone-derived apparent elasticity estimates were significantly higher than sphere-derived estimates across multiple indentation forces ($p < 0.001$).

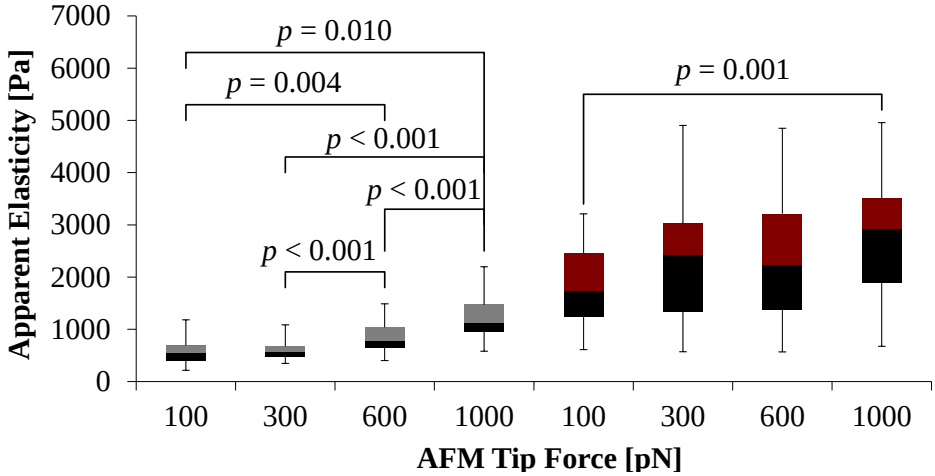

Figure 14: Dependence of elasticity and indentation depth on force for spherical and pyramidal probes at 1.88 μm/s.

Discussion

Importance of Contact Point Detection and Challenges for Data Comparison

One of the central objectives of this work was to develop a new method for processing AFM nanoindentation data that would reliably produce an apparent Young's modulus for the material being tested. The method that was developed relies on several key parameters to complete this task: local maximum threshold, local slope threshold, and scan distance (**Figure 8**). Tuning these parameters, for example by changing the local maximum and local slope thresholds, changes the detected contact point. This tuning process is significant because seemingly minor variations in the detected contact point can give rise to significantly different calculated apparent elasticities after least-squares fitting of a constitutive contact mechanics relation (Equation 1 or 2). This fit is strongly dependent on the choice of the point where the fit begins and errors in contact point selection can increase apparent elasticity a factor of up to 3. This strong sensitivity to the robustness of numerical analysis technique is completely independent of other experimental factors and represents a potential source of error in the absolute magnitude of the apparent modulus that may be biologically, in addition to statistically, significant.

Recent papers have documented the influence of contact point selection on apparent elasticity[9,15]. Unfortunately, correctly determining the contact point is a difficult task[12]. The main difficulties in determining the contact point include characteristic noise in data collection, data features caused by probing cellular organelles, and the volume of data recorded[9]. Despite the difficulty and importance of this task, the numerical analysis method for processing data is treated like a black box in most published articles on this topic.

Ironically, most researchers thoroughly explain their cell culturing and plating techniques and any treatments applied to their cells, but omit a detailed description of how they determine contact point prior to application of a Hertz or Sneddon fit[6,16–18]. In contrast, we have shown that the numerical method should not be seen as of secondary importance to the experimental conditions and may in some cases introduce a source of variation that is as large or larger than the observed treatment effects between groups.

Some authors have introduced methods for determining the contact point by means of multiparameter empirical fits. For example, Gavara's 2016 Nature paper analyzes several parameters to automate contact point detection, these parameters being goodness of it (GoF), ratio of variances (RoV), changes in estimated Young's Modulus, power law exponent (PLE), and the product of combinations of these parameters after normalization[21]. The paper concludes that the product of 3 of these parameters gives the best contact point based on variance, covariance, skewness, and "success rate", where the elasticity falls within a prescribed range. One limitation of this general approach is that adding more parameters can improve the overall goodness-of-fit of a curve to a specific data set, but may also limit the applicability of that fit to other data sets, and can decrease the ability to offer a physical interpretation of each individual parameter. In addition, the existing AFM nanoindentation literature overwhelmingly favors the use of single-parameter Hertz and Sneddon fits for estimating cell elasticity.

Another challenge in interpreting the AFM nanoindentation literature in light of the methods used for data processing is that in many studies, it is unclear whether or not data has been reviewed to ensure that all included raw data are from clean indentations curves. In any experimental AFM series there will inevitably be occasional spurious indentations

that occur as a result of issues such as optical interference, organelle contact, organelle slip, and accidental dish contact (**Figure 15**). These spurious indentations should ideally be flagged and pre-screened during data analysis, or if not, then identified subsequently by the use of robust statistical analysis with outlier identification. Existing literature on this topic is usually vague or silent on the methods used for quality checking and this introduces uncertainty, especially when summary statistics are reported as means, rather than medians, which may amplify the effect of outliers on the summary parameter reported.

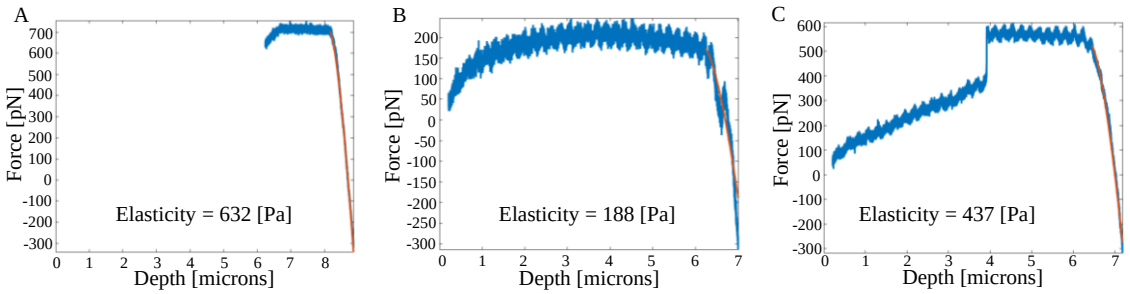

Figure 15: Spurious scans where the probe hits the dish (A), contacts and slides off an organelle during indentation (B), or experiences thermal/optical interference (C).

The overall lack of clarity in data analysis methods for AFM nanoindentation presents a significant obstacle for the research community due to differences in experimental parameters and analysis methods. Probe shape, cell type, and indentation force all have a large effect on elasticity, but even if these parameters are consistent between research groups, different data analysis methods can produce internally consistent elasticity values that have an absolute magnitude much higher and lower than other research groups using different analysis methods. This suggests a strong need for transparency and harmonization among investigators using AFM nanoindentation to study cell mechanics, which may improve the ability to compare reported results between research groups and enhance the pace of discovery.

Key Findings from Test Data Series

As a test of robustness and to measure the relative effects of experimental setup variations, the numerical method described above was applied to a large series of AFM nanoindentation of AsPC-1 cells. In this series, the AFM piezo speed, target tip force, and probe tip shape were varied and the resulting data was processed using the newly written analysis code. For the range of actuation speeds tested, there were no statistically significant effects and no observable trends between speed and apparent elasticity. This finding may be due to the fact that the range of indentation speeds used was fairly narrow, especially by comparison to the breadth of speeds used in frequency-sweeping techniques used to fit viscoelastic material models[2,12,19,20]. This suggests that for AFM nanoindentation, the choice of speed over the typical range used is not a significant source of variation between results reported by different groups with different setups. For experiments conducted a much higher or lower speeds, stronger speed effects may become apparent.

Pyramidal and spherical probe-derived elasticity measurements were statistically different, with pyramidal measurements being up to a factor of 3 larger than spherical measurements. Indentation force also significantly changed apparent elasticity (**Figure 14**), increasing measured elasticity by 100% at the highest indentation value. This method confirms the dependence of apparent elasticity based on both probe shape used and indentation depth/force, as seen in other works, and highlights the need for further research into determining conversion factors to compare data acquired using techniques with different cell lines, probe shapes, and indentation forces, depths, and locations.

One final important implication of this analysis pertains to the statistical distribution of apparent elasticity values produced for a given experimental condition. Previously, multiple investigators have reported that AFM nanoindentation data tends to produce apparent elasticities that are log-normally distributed[2,5]. In comparison, the elasticity data sets produced by this method tend to be much less skewed, with many groups passing Kolmogorov-Smirnov and Shapiro-Wilk normality tests. This implies that the use of the proposed method for contact point detection and manual review to remove any nonphysical scans minimizes the effect of outliers and reduces the tendency toward log-normal distributions that are present in other data sets. A similar effect of different data processing methods on the distribution of elasticity values for a given experiment has been document by other investigators[21]. Our findings suggest that data distributions, not just summary statistics, should be routinely reported in AFM nanoindentation publications.

Conclusions

In this work, a new method for processing AFM nanoindentation data has been developed and tested for robustness. The results suggest that accurate selection of the first point of contact between the nanoindenter and cell surface is essential for accurate data processing. Selecting this point too late can significantly skew the apparent reported elasticity of the cell by a factor of 3. Data checking features designed to facilitate rapid screening of large data sets for spurious individual indentation are also important for ensuring final sample quality and avoiding log-normally distributed summary parameters. Standardization of methods for determining contact point and manual or semi-automatic review of data are both likely to help remove data discrepancies currently present in the

literature. The newly developed method was also tested on a representative AFM nanoindentation data set, leading to the following conclusions. First, over the range of actuation speeds typically used in AFM, speed does not significantly influence the apparent elasticity of the material. The use of higher indentation forces and pyramidal versus spherical probes each resulted in significantly higher apparent elasticities. The relative magnitude of these effects was 3x for using a pyramidal probe and 2x for using the highest indentation force. Inclusion of distributions of indentation depth, measured indentation force, number of nonphysical scans, apparent elasticities, and all raw data may also improve collaboration and clarity between research groups and confirm validity of contact models used in deriving elasticity. Finally, to test the robustness of data processing methods and to further address limitations of violating underlying assumptions, experiments should be performed on more controlled model systems. For example, using hydrogels rather than cells would eliminate boundary effects and the influence of structural inhomogeneities that are inherent in cellular elasticity measurements.

References

1. Lekka, M. *et al.* Elasticity of normal and cancerous human bladder cells studied by scanning force microscopy. *Eur. Biophys. J.* **28,** 312–316 (1999).

2. Efremov, Y. M. *et al.* The effects of confluency on cell mechanical properties. *J. Biomech.* (2013). doi:10.1016/j.jbiomech.2013.01.022

3. Lekka, M. Atomic force microscopy: A tip for diagnosing cancer. *Nat. Nanotechnol.* **7,** 691–692 (2012).

4. Costa, K. D., Sim, A. J. & Yin, F. C.-P. Non-Hertzian Approach to Analyzing Mechanical Properties of Endothelial Cells Probed by Atomic Force Microscopy. *J. Biomech. Eng.* **128,** 176 (2006).

5. Efremov, Y. M. *et al.* Distinct impact of targeted actin cytoskeleton reorganization on mechanical properties of normal and malignant cells. *Biochim. Biophys. Acta - Mol. Cell Res.* **1853,** 3117–3125 (2015).

6. Cross, S. E., Jin, Y.-S., Rao, J. & Gimzewski, J. K. Nanomechanical analysis of cells from cancer patients Change in cell stiffness is a new characteristic of cancer cells that affects the way they spread 1,2 . Despite several studies on architectural changes in cultured cell lines. (2007). doi:10.1038/nnano.2007.388

7. Babahosseini, H., Carmichael, B., Strobl, J. S., Mahmoodi, S. N. & Agah, M. Sub-cellular force microscopy in single normal and cancer cells. *Biochem. Biophys. Res. Commun.* **463,** 587–592 (2015).

8. Li, Q. S., Lee, G. Y. H., Ong, C. N. & Lim, C. T. AFM indentation study of breast cancer cells. *Biochem. Biophys. Res. Commun.* **374,** 609–613 (2008).

9. Costa, K. D. Single-cell elastography: Probing for disease with the atomic force microscope. *Dis. Markers* **19,** 139–154 (2003).

10. Butt, H. J., Cappella, B. & Kappl, M. Force measurements with the atomic force microscope: Technique, interpretation and applications. *Surf. Sci. Rep.* (2005). doi:10.1016/j.surfrep.2005.08.003

11. Nawaz, S. *et al.* Cell Visco-Elasticity Measured with AFM and Optical Trapping at Sub-Micrometer Deformations. *PLoS One* (2012). doi:10.1371/journal.pone.0045297

12. Stolz, M. *et al.* Dynamic Elastic Modulus of Porcine Articular Cartilage Determined at Two Different Levels of Tissue Organization by Indentation-Type Atomic Force Microscopy. *Biophys. J.* **86,** 3269–3283

13. Hertz, H. Ueber die Beruehrung fester elastischer Koerper. *J. für die reine und Angew. Math.* **92,** 156–171 (1882).

14. Sneddon, I. N. The relation between load and penetration in the axisymmetric boussinesq problem for a punch of arbitrary profile. *Int. J. Eng. Sci.* **3,** 47–57 (1965).

15. Gavara, N. & Chadwick, R. S. Determination of the elastic moduli of thin samples and adherent cells using conical atomic force microscope tips. (2012). doi:10.1038/NNANO.2012.163

16. Darling, E. M., Zauscher, S. & Guilak, F. Viscoelastic properties of zonal articular chondrocytes measured by atomic force microscopy. *Osteoarthr. Cartil.* (2006). doi:10.1016/j.joca.2005.12.003

17. Dimitriadis, E. K., Horkay, F., Maresca, J., Kachar, B. & Chadwick, R. S. Determination of Elastic Moduli of Thin Layers of Soft Material Using the Atomic Force Microscope. *Biophys. J.* **82,** 2798–2810

18. Efremov, Y. M., Wang, W.-H., Hardy, S. D., Geahlen, R. L. & Raman, A. Measuring nanoscale viscoelastic parameters of cells directly from AFM force-displacement curves. *Sci. Rep.* (2017). doi:10.1038/s41598-017-01784-3

19. Smith, B. A., Tolloczko, B., Martin, J. G. & Grü, P. Probing the Viscoelastic Behavior of Cultured Airway Smooth Muscle Cells with Atomic Force Microscopy: Stiffening Induced by Contractile Agonist. *Biophys. J.* **88,** 2994–3007

20. Alcaraz, J. *et al.* Microrheology of Human Lung Epithelial Cells Measured by Atomic Force Microscopy. *Biophys. J.* **84,** 2071–2079 (2003).

21. Gavara, N. Combined strategies for optimal detection of the contact point in AFM force-indentation curves obtained on thin samples and adherent cells. *Sci. Rep.* **6,** (2016).

Appendix A: Detailed Experimental Methods

In preparation for indentation, the AFM was calibrated using the in PBS solution to obtain the spring constant and the inverse optical laser sensitivity value. During a nanoindentation scan, the AFM tip travels vertically towards the bEnd.3 surface. Upon indentation of the cell, the AFM cantilever acts like a soft spring and deflects. The cantilever deflection is measured and plotted as a function of sample position along the z axis (**Figure 1**, **Figure 16**). The slope of this force-indentation curve directly reflects the cell stiffness (expressed in [pN/nm]), but can be converted to an apparent material stiffness, E, in [Pa] by means of equations derived from classical contact mechanics for a sphere (Hertz equation) or cone (Sneddon equation) in contact with a semi-infinite medium.

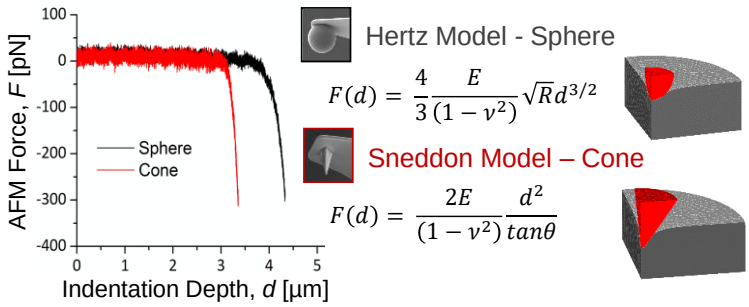

Figure 16: Representative AFM force-indentation curves for a spherical and conical probe and the contact mechanics equations used to infer cell stiffness from experiments with spherical and conical probes.

To characterize the effect of experimental parameters on the apparent cell stiffness inferred from AFM measurements, AsPC-1 (human pancreatic adenocarcinoma) cells were passaged and incubated with Dulbecco's Modified Eagle's Medium (DMEM) in 35-mm culture dishes for 24 hours prior to experimentation. The following four experimental variables were considered:

- AFM Tip Shape – conical vs. 5-µm diameter spherical tip
- Piezo Actuation Speed – 0.94, 1.88, 3.76, and 7.52 µm/s
- Peak Indentation Force – 100, 300, 600, and 1000 pN
- Indentation Location – cell nucleus

For each indentation, apparent cell stiffness was calculated using equations derived from classical contact mechanics with the Hertz model for the spherical tip and Sneddon model for the cone (**Figure 1**, **Figure 16**). Twenty indentations were performed for each cell at each location (nucleus, periphery) and experimental condition was repeated for 40 cells.

Appendix B: Hertz and Sneddon Contact Models

Hertz Model

In contact problems without friction, the z-component is the only one of interest (**Figure 2**). The radius of the contact area can be approximated, based on a geometric derivation, as

$$a = \sqrt{Rd} \tag{3}$$

where R is the radius of the sphere, d is the depth, and a is the contact area.

The apparent young's modulus in this case is

$$\frac{1}{E^*} = \left(\frac{1-\nu_1^2}{E_1} + \frac{1-\nu_2^2}{E_2}\right) \tag{4}$$

Where E_1 is the elasticity of the cell and E_2 is the elasticity of the sphere. In this case, the elasticity of the sphere is much larger than that of the cell, and this reduces to

$$\frac{1}{E^*} = \left(\frac{1-\nu_1^2}{E_1}\right) \tag{5}$$

For contact between a rigid solid and an elastic solid, the Hertzian pressure distribution, assuming pressure is exerted in a circle, is

$$P(r) = P_0\left(1 - \frac{r^2}{a^2}\right)^{1/2} \tag{6}$$

where P_0 is the maximum pressure, given by

$$P_0 = \frac{3F}{2\pi a^2} = \frac{1}{\pi}\left(\frac{6FE^{*2}}{R^2}\right)^{1/3} \tag{7}$$

According to contact equations between a sphere and an elastic half space, the radius of the circle is related to the applied load F by the equation

$$a^3 = \frac{3FR}{4E^*} \tag{8}$$

and the depth of indentation d is related to the maximum contact pressure by

$$d = \frac{a^2}{R} = \left(\frac{9F^2}{16E^{*2}R}\right)^{1/3} \tag{9}$$

Rearranging this equation produces relation that can be used to fit apparent material elasticity, E_{app}, from the experimentally acquired force and indentation depth data:

$$E_{app} = \frac{3}{4}\frac{(1-\nu^2)F}{R^{1/2}d^{3/2}} \tag{10}$$

Sneddon Model

In contact problems without friction, the z-component is the only one of interest (**Figure 3**). The total indentation depth is related to the area of contact by

$$a = \frac{2}{\pi} d \tan\theta \tag{11}$$

The contact pressure is given by

$$P(r) = -\frac{Ed}{\pi a(1-\nu^2)} \ln\left(\frac{a}{r} + \sqrt{\left(\frac{a}{r}\right)^2 - 1}\right) = \frac{Ed}{\pi a(1-\nu^2)} \cosh^{-1}\left(\frac{a}{r}\right) \tag{12}$$

The pressure has a singularity at the tip of the cone and after integrating over the area, the total force is given as

$$F = \frac{\pi E}{2(1-\nu^2)} a^2 \tan\theta = \frac{2E}{\pi(1-\nu^2)} \frac{d^2}{\tan\theta} \tag{13}$$

As before, rearranging this equation produces relation that can be used to fit apparent material elasticity, E_{app}, from the experimentally acquired force and indentation depth data:

$$E_{app} = F\pi \frac{(1-\nu^2)\tan\theta}{2d^2} \tag{14}$$

Despite the wide use of these models in AFM data analysis, several of the underlying assumptions are intrinsically violated in the AFM experiment. Small strain assumptions are likely to be invalid, but strains are not directly measured, and in most experiments, nanoindentation does not cause cell rupture and death. Some authors have proposed neo-Hookean nonlinear material models, but this work presents the numerical analysis technique in the context of the ubiquitous linear-elastic Hertz and Sneddon models. In addition, the assumptions of small contact area and semi-infinite contacted body are universally violated in AFM experiments, with most authors reporting indentations ranging from 1 to 10 microns or more for cell bodies that are typically 2 to 8 microns tall. The frictionless contact assumption is difficult to validate, although experiments on living cells are done in cell medium, which may be expected to produce relatively low friction between the cell surface and AFM tip. Despite these significant limitations, the Hertz- and Sneddon-based data analysis is widely used in the field, and is retained for this work.

Vita

Jared Feindt was born December 1st, 1993 in Newark, Delaware to his parents Joseph and Joanne Feindt. Jared attended Woodstown High school where he graduated in 2012. He received his Bachelor's Degree in Biomedical Engineering from Bucknell University in 2016. As an undergraduate, Jared was a part of the Biomedical Engineering Society and Tau Beta Pi (Engineering Honor Society). Jared went on to get his Masters of Science Degree in Mechanical Engineering from Lehigh University in 2017. As a graduate student, Jared was awarded a Mechanical Engineering and Mechanics Departmental fellowship for one semester, and acted as a Research Assistant under his advisor, Dr. Hannah Dailey, for one semester. Jared was also a graduate student mentor for two summers on the BDSI Zhang/Dailey team in 2016 and 2017. Jared is currently pursuing job opportunities in medical device engineering, engineering consulting, and healthcare consulting fields.